Commun Nonlinear Sci Numer Simulat 15 (2010) 1092–1102

Contents lists available at ScienceDirect

Commun Nonlinear Sci Numer Simulat

journal homepage: www.elsevier.com/locate/cnsns

On the dynamical properties of an elliptical–oval billiard with static boundary

Diego F.M. Oliveira [a,*], Edson D. Leonel [b]

[a] Departamento de Física, Instituto de Geociências e Ciências Exatas, Universidade Estadual Paulista, Av. 24A, 1515, Bela Vista, CEP: 13506-900, Rio Claro, SP, Brazil
[b] Departamento de Estatística, Matemática Aplicada e Computação, Instituto de Geociências e Ciências Exatas, Universidade Estadual Paulista, Av. 24A, 1515, Bela Vista, CEP: 13506-900, Rio Claro, SP, Brazil

ARTICLE INFO

Article history:
Received 7 May 2009
Accepted 9 May 2009
Available online 23 May 2009

Keywords:
Billiard
Chaos
Lyapunov

ABSTRACT

Some dynamical properties for a classical particle confined inside a closed region with an elliptical–oval-like shape are studied. The dynamics of the model is made by using a two-dimensional nonlinear mapping. The phase space of the system is of mixed kind and we have found the condition that breaks the invariant spanning curves in the phase space. We have discussed also some statistical properties of the phase space and obtained the behaviour of the positive Lyapunov exponent.

1. Introduction

The interest in understanding the dynamics of billiard problems becomes in earlies 1927 when Birkhoff [1] introduced a system to describe the motion of a free particle inside a closed region with which the particle suffers elastic collisions. In general, a billiard is defined by a connected region $Q \subset R^D$, with boundary $\partial Q \subset R^{D-1}$ which separates Q from its complement. Inside the billiard, a point particle of mass m (commonly it is assumed to be the unity) moves freely along a straight line until it encounters the boundary. After the collision, it is assumed that the particle is specularly reflected. It thus implies that the incidence angle must be equals to the reflection angle. It is well known that depending on the shape of the boundary as well as on the combination of both control parameters and initial conditions, the dynamics of the particle might generate phase spaces of different kinds, including: (i) regular; (ii) ergodic; (iii) mixed. The integrability of the regular cases is generally related to some kind of preservation in the dynamics, in particular the angular momentum. On the other hand, for the completely ergodic billiards, only chaotic and therefore unstable periodic orbits are present in the dynamics. In order to illustrate systems that show such property, the so called Bunimovich stadium [2,3] and the Sinai billiard [4,5] consist of typical examples. For these systems the time evolution of a single initial condition, for appropriated combinations of control parameters, is enough to fills up ergodically the entire phase space. Finally, there is a representative number of billiards that present mixed phase space structure [6–12], which have control parameters with different physical significance.

Depending on the combination of both the initial conditions and control parameters, the phase space presents a very rich structure which could, in principle, contains invariant spanning curves (sometimes also called as invariant tori), Kolmogorov–Arnold–Moser (KAM) islands and chaotic seas. This mixed structure of the phase space is generic for non-degenerate Hamiltonian systems [13] and might be observed in problems of one-dimensional time-dependent potentials [14–18], rippled channels [19,20] and many other different problems including tokamak [21–23].

* Corresponding author.
E-mail addresses: dfmo@rc.unesp.br (D.F.M. Oliveira), edleonel@rc.unesp.br (E.D. Leonel).

1007-5704/$ - see front matter © 2009 Elsevier B.V. All rights reserved.
doi:10.1016/j.cnsns.2009.05.044

In this paper, we propose a special geometry for the boundary of a classical billiard, which we call as elliptical–oval boundary. Our main goal is to understand and describe some dynamical and moreover chaotic properties of such system. It is important to say that the shape of the boundary is controlled by three relevant control parameters. Varying such parameters we can recover the results of the circular billiard and elliptical billiard, the oval billiard and finally we obtain totally new results considering simultaneously variation of both control parameters, thus having an elliptical–oval billiard shape.

In the first part of this paper, we discuss all the details needed to construct the mapping that describes the dynamics of the model. The shape of the boundary is dependent on three control parameters and its expression in polar coordinates is given by $R(\theta,p,e,\epsilon)=(1-e^2)/(1+e\cos(\theta))+\epsilon\cos(p\theta)$, where p is an integer number, e and ϵ are parameters that control the circle deformation. Inside the boundary, we consider that a classical particle of mass m is moving freely and in the total absence of any external field. When the particle hits the boundary it changes the direction according to a specular reflection without suffering fractional loss of energy. The phase space is mixed, in the sense that, depending on both, the combination of the control parameters and initial conditions, KAM islands usually surrounded by a chaotic sea, limited by a set of invariant spanning curves, can be observed. We have found a critical control parameter where no invariant spanning curves are observed. This condition is related to the fact that the boundary may changes locally from positive curvature to negative curvature. After constructing the mapping, we explore some numerical results from it. For the case of $e=\epsilon=0$, we recover the results of the circular billiard where only regular dynamics is observed in the phase space. Considering the situation where $\epsilon=0$ and $e\neq 0$, then the results for the elliptical billiard are obtained. If we assume that $e=0$ and $\epsilon\neq 0$, we obtain the results for the oval billiard. The last case is assuming that $e\neq 0$ and $\epsilon\neq 0$.

For the second part of the paper, we obtain and discuss some numerical results for the four possible cases, as discussed above. We show that the positive Lyapunov exponent grows as the control parameters increase and it passes a regime of maximum then experiencing a small decay. We explain the increase in the Lyapunov exponent based on the behaviour of the histogram of frequency for chaotic orbits.

The paper is organized as follows: in Section 2 we give all the details needed for the construction of the nonlinear mapping that describes the dynamics of the elliptical–oval billiard. Section 3 is devoted to discuss our numerical results and dynamical properties of the system as function of the control parameters. Finally, in Section 4 we drawn our conclusions.

2. The elliptical–oval billiard and the mapping

In this section we discuss all the details needed for the construction of a nonlinear map that describes the dynamics of the problem. The model consists basically in consider the dynamics of a classical particle of mass m confined into a closed region suffering elastic and specular collisions with the border. When the particle hits the boundary it is reflected with the same velocity. The radius of the boundary, in polar coordinates, is given by

$$R(\theta,p,e,\epsilon)=\left[\frac{1-e^2}{1+e\cos(\theta)}\right]+\epsilon\cos(p\theta). \tag{1}$$

The control parameter $e\in[0,1)$ controls the deformation of the circle thus recovering circle and elliptical shapes. The control parameter $\epsilon\in[0,1)$ also controls a circle deformation thus recovering oval shapes. p is an integer number and $\theta\in[0,2\pi)$ is a counterclockwised angle measured with respect to the positive horizontal axis. For the case $e=\epsilon=0$, we recover the circular boundary. If $e\neq 0$ and $\epsilon=0$ we have the elliptical boundary. For the case of $e=0$ and $\epsilon\neq 0$, we obtain the oval shape boundary and finally for the case of $e\neq 0$ and $\epsilon\neq 0$ we obtain the elliptical–oval-like shape boundary. It is shown in Fig. 1 the geometry of the boundary for different values of control parameters e, ϵ and p.

As it is usual in the literature, the dynamics of the particle is described in terms of a two-dimensional nonlinear mapping $T(\theta_n,\alpha_n)=(\theta_{n+1},\alpha_{n+1})$ where the dynamical variable θ_n denotes the angular position of the particle when it hits the border. α_n is the angle that the trajectory does with the tangent vector to the border at the angular position θ_n (the illustrations of these angles are made in Fig. 2). The index n denotes the nth collision of the particle with the boundary. Using polar coordinates, we can find the expressions for both $X(\theta_n)$ and $Y(\theta_n)$ as

$$X(\theta_n)=\left[\frac{1-e^2}{1+e\cos(\theta_n)}+\epsilon\cos(p\theta_n)\right]\cos(\theta_n), \tag{2}$$

$$Y(\theta_n)=\left[\frac{1-e^2}{1+e\cos(\theta_n)}+\epsilon\cos(p\theta_n)\right]\sin(\theta_n). \tag{3}$$

Given an initial condition (θ_n,α_n), the angle between the tangent and the boundary at the position $X(\theta_n)$ and $Y(\theta_n)$ is

$$\phi_n=\arctan\left[\frac{Y'(\theta_n)}{X'(\theta_n)}\right], \tag{4}$$

where the expressions for both $X'(\theta_n)$ and $Y'(\theta_n)$ are written as

$$X'(\theta_n)=\frac{dR(\theta_n)}{d\theta_n}\cos(\theta_n)-R(\theta_n)\sin(\theta_n), \tag{5}$$

$$Y'(\theta_n)=\frac{dR(\theta_n)}{d\theta_n}\sin(\theta_n)+R(\theta_n)\cos(\theta_n). \tag{6}$$

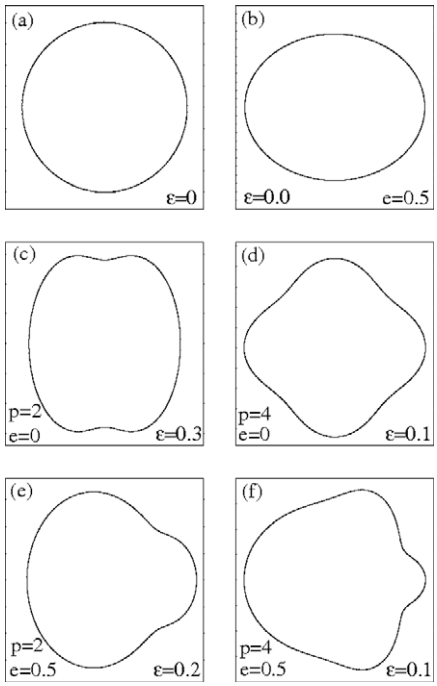

Fig. 1. Shapes of the boundaries for different combinations of control parameters, as shown in the figure.

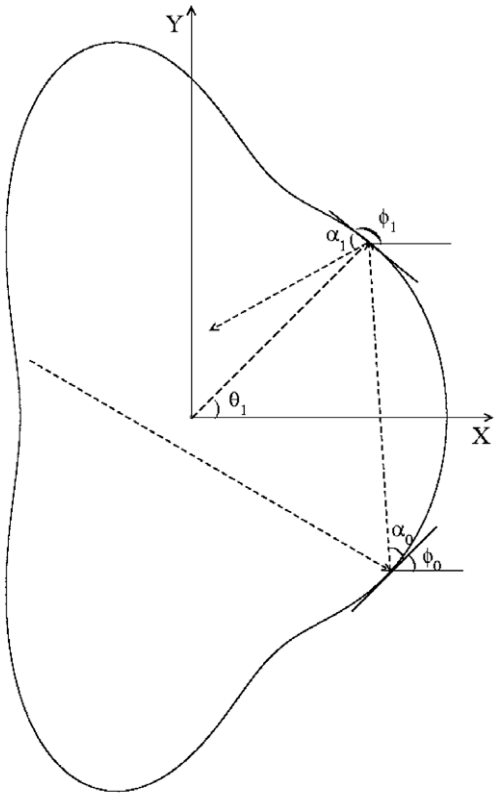

Fig. 2. Illustration of a particle's trajectory.

The term $dR(\theta_n)/d\theta_n$ is given by

$$\frac{dR(\theta_n)}{d\theta_n} = \frac{(1-e^2)e\sin(\theta_n)}{[1+e\cos(\theta_n)]^2} - \epsilon p \sin(p\theta_n). \tag{7}$$

We stress that the particle does not suffers influence of any external field upon collisions with the boundary. The particle thus travels with constant velocity along a straight line until reaches the boundary. To obtain the new angular position for the next hit of the particle with the border, we must solve the following equation

$$Y(\theta_{n+1}) - Y(\theta_n) = \tan(\alpha_n + \phi_n)[X(\theta_{n+1}) - X(\theta_n)], \tag{8}$$

where ϕ_n is obtained from the slope between the tangent vector and the positive horizontal axis. $X(\theta_{n+1})$ and $Y(\theta_{n+1})$ are the new positions of the particle at the angular position θ_{n+1}, which is numerically obtained as solution of Eq. (8). The new angle that the trajectory does with the tangent at θ_{n+1} is obtained from geometrical considerations, as can be seen in Fig. 2. It is given by

$$\alpha_{n+1} = \phi_{n+1} - (\alpha_n + \phi_n). \tag{9}$$

Fig. 2 illustrates geometrically all the details needed to obtain the new angle α_{n+1}. Thus, we obtain that the map which describes the dynamics of the model is given by

$$T: \begin{cases} F(\theta_{n+1}) = R(\theta_{n+1})\sin(\theta_{n+1}) - Y(\theta_n) - \tan(\alpha_n + \phi_n)[R(\theta_{n+1})\cos(\theta_{n+1}) - X(\theta_n)], \\ \alpha_{n+1} = \phi_{n+1} - (\alpha_n + \phi_n) \end{cases} \tag{10}$$

where θ_{n+1} is numerically obtained as the solution of $F(\theta_{n+1}) = 0$, $R(\theta_{n+1}) = (1-e^2)/(1+e\cos(\theta_{n+1})) + \epsilon\cos(p\theta_{n+1})$ and $\phi_{n+1} = \arctan[Y'(\theta_{n+1})/X'(\theta_{n+1})]$.

3. Numerical results

Let us now present and discuss some of our results. To illustrate the behaviour of the phase space for some of the possible combinations of control parameters, we shown in Fig. 3, the phase space generated by iterating the Eq. (10) for: (a) $e = \epsilon = 0$ and (b) $e = 0.5$ and $\epsilon = 0$. For case (a) we can see both straight lines (quasi-periodic behaviour) in the phase space and

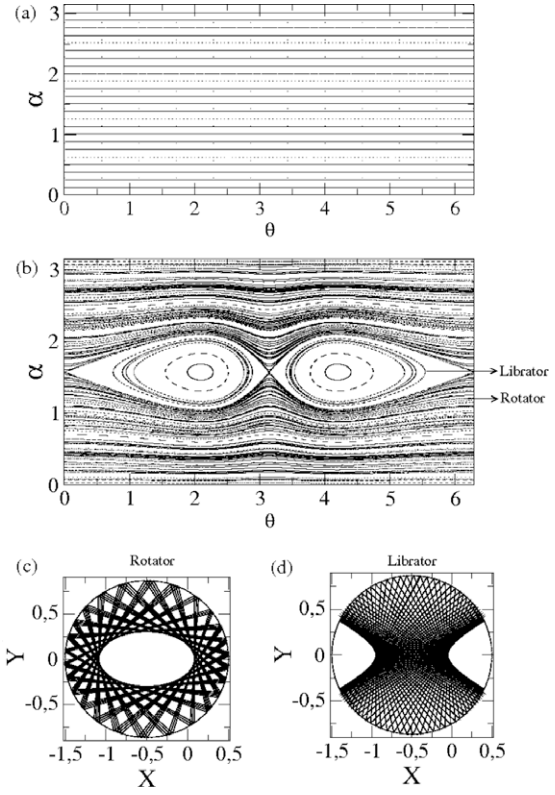

Fig. 3. Phase space for the elliptical–oval billiard considering the control parameters: (a) $e = \epsilon = 0$, (b) $e = 0.5$ and $\epsilon = 0$, (c) a rotator orbit and (d) a librator orbit.

periodic orbits marked by a finite set of points in the phase portrait, as it is known from the circular billiard [6,24]. On the other hand, for (b) we can see a large double island limited by a separatrix curve and a set of invariant spanning curves, thus recovering results of the elliptical phase space as it is well known in the literature [6,25]. In Fig. 3(b) we can observe two different kinds of behaviour in the phase space separated by a separatrix, namely, rotators and librators. Librators consist of trajectories that are confined between the two focus and in the phase space are confined into the separatrix curve. On the other hand, rotators are trajectories near to the boundary exploring all the values of θ. In the phase space they are outside of the separatrix curve. Fig. 3(c, d) shows the behaviour of both, rotators and librators, respectively.

If we consider the case with $e = 0$ and $\epsilon \neq 0$, as shown in Fig. 4 we can see a complex hierarchy of behaviours in the phase space including a large chaotic sea. The control parameters used in the construction of Fig. 4 were (a) $\epsilon = 0.1$ and $p = 2$; (b) $\epsilon = 0.05$ and $p = 3$. It is also easy to see the presence of invariant spanning curves. Therefore, if we increase the control parameter slightly above the condition

$$\epsilon_c = \frac{1}{1+p^2}, \quad p \geqslant 1, \tag{11}$$

all the invariant spanning curves are destroyed. The explanation for such kind of destruction is related to the shape of the boundary, thus now presenting some regions of nonconvex curvature. If we consider $\epsilon < \epsilon_c$ the boundary is convex, however, if $\epsilon > \epsilon_c$ we can observe nonconvex structure on the boundary (for more details see Appendix). To illustrate the absence of the invariant spanning curves in the phase space, it is shown in Fig. 5 the phase space for the following combinations of control parameters: $e = 0$ and (a) $\epsilon = 0.21$ and $p = 2$; (b) $\epsilon = 0.11$ and $p = 3$.

An important property regarding the chaotic sea that must be discussed is the behaviour of the positive Lyapunov exponent. It is well known that the Lyapunov exponent has a great applicability as a practical tool that can quantify the average expansion or contraction rate for a small volume of initial conditions. As discussed in [26], the Lyapunov exponents are defined as

$$\lambda_j = \lim_{n\to\infty} \frac{1}{n} \ln |\Lambda_j|, \quad j = 1, 2, \tag{12}$$

where Λ_j are the eigenvalues of $M = \prod_{i=1}^{n} J_i(\alpha_i, \theta_i)$ and J_i is the Jacobian matrix evaluated over the orbit (α_i, θ_i). In order to illustrate that the oval billiard has a chaotic component in the phase space, we shown in Fig. 6 the behaviour of the positive Lyapunov exponent as function of the number of collisions of the particle with the boundary for 5 different initial conditions both chosen on the chaotic sea. Each initial condition was iterated up to 10^8 times. As we see in Fig. 6(a) one of the time

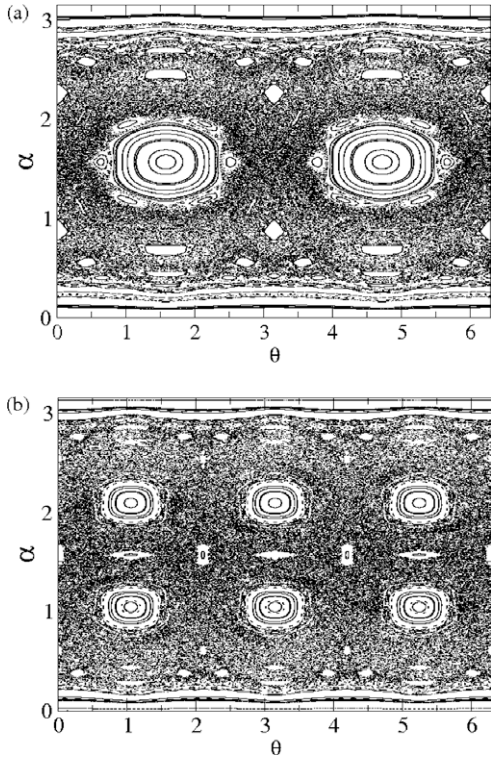

Fig. 4. Phase space for the oval billiard. The control parameters used in the construction of the figures were: (a) $\epsilon = 0.1$ and $p = 2$; (b) $\epsilon = 0.05$ and $p = 3$.

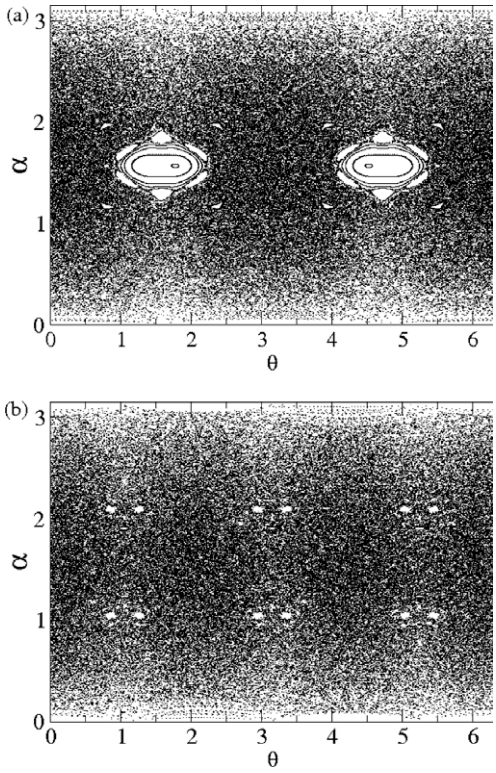

Fig. 5. Phase space for the oval billiard. The control parameters used in the construction of the figures were: (a) $\epsilon = 0.21$ and $p = 2$; (b) $\epsilon = 0.11$ and $p = 3$. As one can see the invariant spanning curves were destroyed.

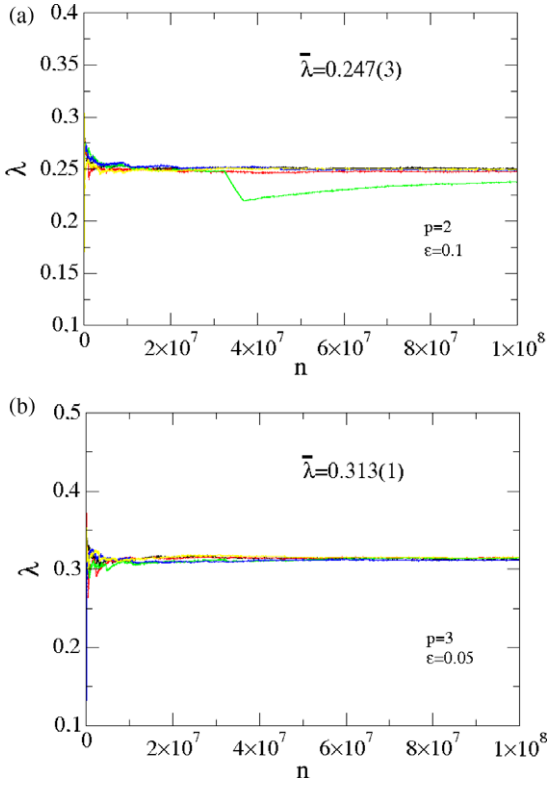

Fig. 6. Convergency of the positive Lyapunov exponent for the oval billiard. The control parameters used in the figure were (a) $\epsilon = 0.1$ and $p = 2$, (b) $\epsilon = 0.05$ and $p = 3$.

series suffers a small decay for approximately 4.5×10^6 collisions with the boundary. After that, the positive Lyapunov exponent tends towards a regime of convergency marked by a constant plateau. The short decay is due to the fact that the particle has been confined into a sticky region by around 4.5×10^6 iterations. The control parameters used in the construction of Fig. 6(a) were $\epsilon = 0.1$ and $p = 2$ and (b) $\epsilon = 0.05$ and $p = 3$. The average of the positive Lyapunov exponent for the ensemble of 5 samples furnishes (a) $\bar{\lambda} = 0.247 \pm 0.003$ and (b) $\bar{\lambda} = 0.313 \pm 0.001$. The values ± 0.003 and ± 0.001 correspond to the standard deviation of the 5 samples.

Let us now present the behaviour of the positive Lyapunov exponent as function of the control parameter ϵ. It is shown in Fig. 7 the behaviour of $\lambda \times \epsilon$ for two values of p, namely (a) $p = 2$ and (b) $p = 3$. The ranges of values for ϵ used were: (a) $\epsilon \in [0.06, 0.40]$ and (b) we considered $\epsilon \in [0.03, 0.18]$. The initial conditions used in the construction of both figures were $\alpha_0 = 0.3$ and θ_0 uniformly distributed in the range of $[0, 2\pi]$. Each point was obtained from the average of 5 different initial conditions. Each initial condition was iterated 10^6 times. The error bars correspond to the standard deviation of the 5 samples. Note however that, contrary to what was expected to be observed, after the destruction of the invariant spanning curves, the positive Lyapunov exponent does not changes suddenly. The arrow in the Fig. 7 indicates the value of the critical parameter ϵ_c.

We can also characterize some properties of the chaotic sea using average quantities along the phase space. We study the behaviour of the average angle $\bar{\alpha}$ as well as the behaviour of the deviation of the average angle, which we call as ω. We define ω as

$$\omega(n, \epsilon) = \frac{1}{M} \sum_{i=1}^{M} \sqrt{\overline{\alpha_i^2}(n, \epsilon) - \bar{\alpha}_i^2(n, \epsilon)}, \tag{13}$$

where the average angle α is obtained using that

$$\bar{\alpha}(n, \epsilon) = \frac{1}{n+1} \sum_{i=0}^{n} \alpha_i. \tag{14}$$

Eq. (13) was iterated using an ensemble of $M = 2 \times 10^3$ different initial conditions chosen along the chaotic sea. Fig. 8(a) shows the behaviour of the average angle $\bar{\alpha}$ as function of n and Fig. 8(b) shows the behaviour of ω as function of n for three different control parameters. It is easy to see in Fig. 8 two different kinds of behaviours. For short iteration number and after a short transient both $\bar{\alpha}$ and ω grow and suddenly they bend towards a regime of saturation for large n. The changeover from

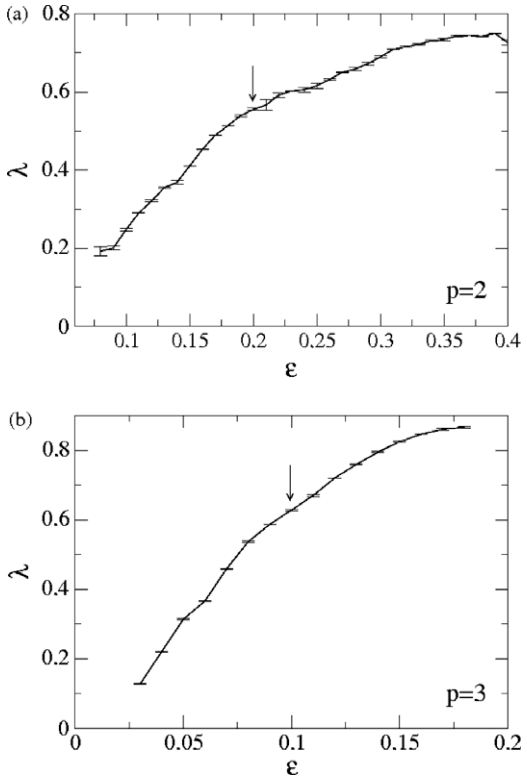

Fig. 7. (a) Behaviour of the Lyapunov Exponent as function of the control parameter ϵ. The control parameter used were (a) $p = 2$ and (b) $p = 3$. The Lyapunov Exponents for the critical value of ϵ are indicate in the figure.

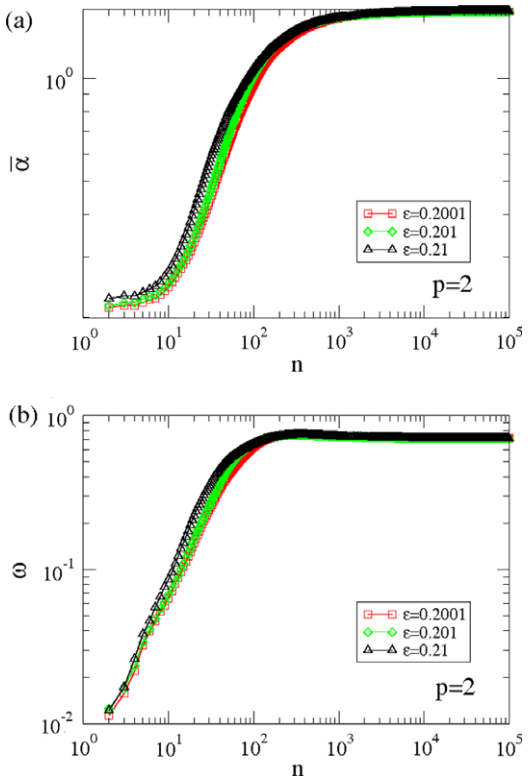

Fig. 8. (a) The average angle $\bar{\alpha}$ as function of n and (b) ω as function of n.

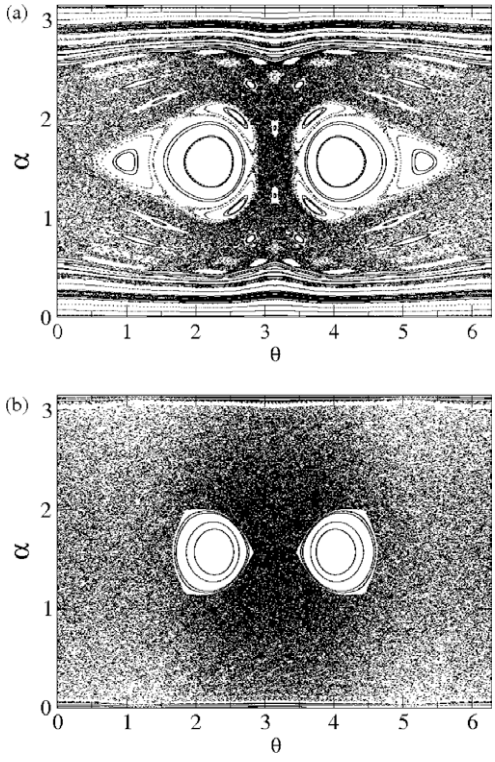

Fig. 9. Phase space for the elliptical–oval billiard. The control parameters used in (a) and (b) were: (a) $\epsilon = 0.01$; (b) $\epsilon = 0.06$ and fixed $p = 2$ and $e = 0.6$. The critical value of ϵ for these control parameters is $\epsilon_c = 0.05$. As one can see, in fig. (b), after the changing of curvature the invariant spanning curves were destroyed.

growth to the saturation is marked by a crossover iteration number n_x. When $n \ll n_x$ the deviation of the average angle grows according to the power law

$$\omega(n,\epsilon) \propto n^{\beta}. \tag{15}$$

After doing some extensive simulation for the range of $\epsilon \in [0.2001, 0.21]$ we obtain that $\beta = 1.23 \pm 0.02$. As n increases, $n \gg n_x$, ω approaches a regime of saturation. However for the range of control parameters we have considered, the plateaus do not seem to depend on the control parameters. Such a property is related to the limited region of the phase space, i.e. $\alpha \in [0, \pi]$ as well as to the symmetry existing in the regions $\alpha \in [0, \pi/2]$ and $\alpha \in [\pi/2, \pi]$.

Let us now consider the elliptical–oval case. We assume that both $e \neq 0$ and $\epsilon \neq 0$. It is shown in Fig. 9(a) the phase space for different values of ϵ and considering fixed the values of e and p, as shown in the figure. We can see that the phase space shows a rich structure of behaviour exhibiting KAM islands surrounded by a chaotic sea and a set of invariant spanning curves. The invariant spanning curves will be destroyed for the case of nonconvex curves. The condition that destroys the invariant spanning curves is given by

$$\epsilon_c = \frac{1-e}{(1+e)(1+p^2)}, \quad p > 1. \tag{16}$$

Considering the case where $\epsilon > \epsilon_c$, all the invariant spanning curves are destroyed, as shown in Fig. 9(b).

As a next step we obtain the behaviour of the positive Lyapunov exponent as function of ϵ as shown in Fig. 10. Fig. 10(a) shows the positive Lyapunov exponent obtained for the chaotic sea using different values for the control parameter e and ϵ. It must be emphasized that different values of the parameter e generate different behaviour for Lyapunov exponent. However, applying the transformation $\epsilon \to \epsilon e^{0.5}$, all the curves grow together as shown in Fig. 10(b). We can see in Fig. 10(a) for a small ϵ, the value of the Lyapunov exponent grows, passing then at a maximum value and experiencing a small decrease. As an attempt to explain the increase in the Lyapunov exponent, we obtain the histogram of frequency for the visited regions in the phase space. We have produced both histograms for the variables α and θ. It is then shown in Fig. 11(a) the histogram of frequency for the control parameters $p = 2$, $e = 0.2$, (a,b) $\epsilon = 0.1$ and (c,d) $\epsilon = 0.4$. We can see that raising the control parameter ϵ, causes a slightly modification to the behaviour of the histogram of frequency for the variable α. However it causes a profound change in the form of the histogram of frequency for the variable θ. Basically there is a small valley for

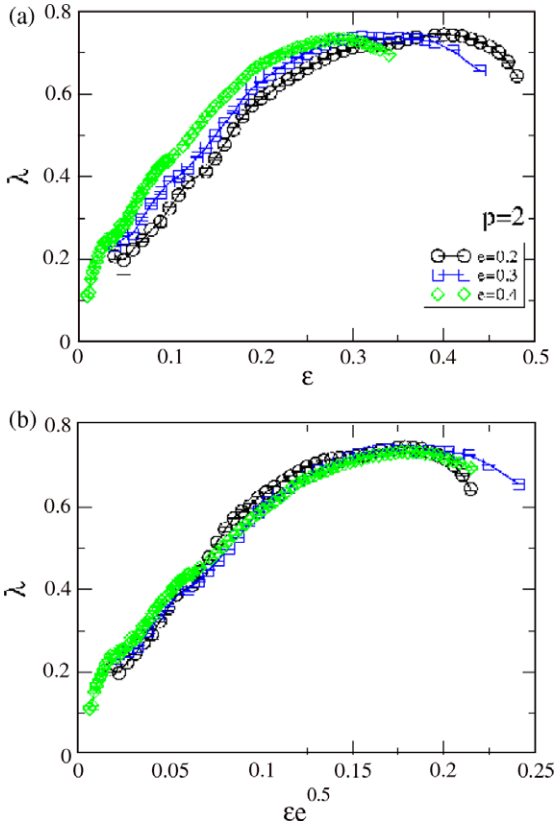

Fig. 10. (a) Behaviour of the Lyapunov Exponent as function of the control parameter ϵ. The control parameter used were (a) $p = 2$ and (b) their collapse after the transformation $\epsilon e^{0.5}$.

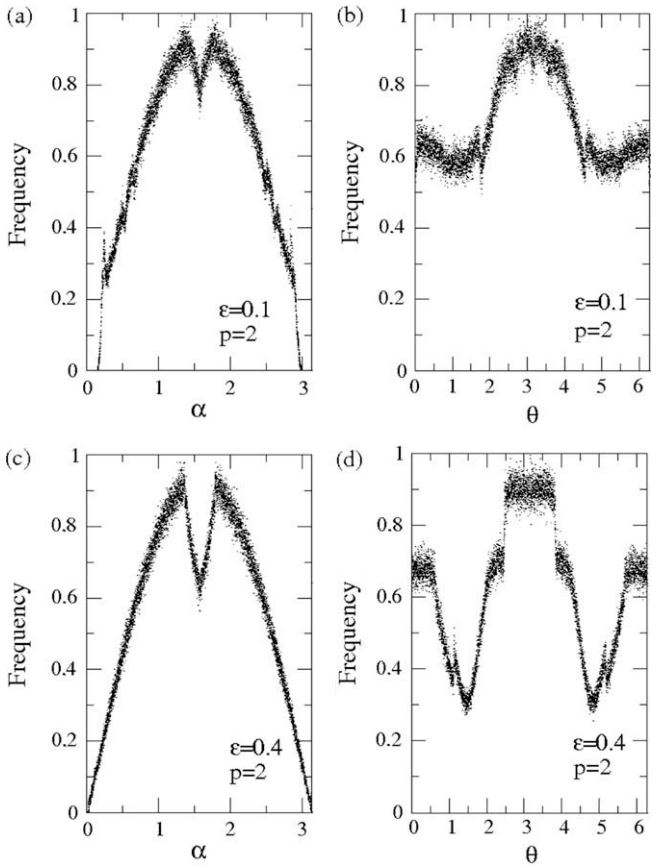

Fig. 11. Histogram of frequency as function of the angles α (a,c) and θ (b and d). The control parameters used were $p = 2$, $e = 0.2$ and (a and b) $\epsilon = 0.1$; (c and d) $\epsilon = 0.4$.

the region around $\alpha = \pi/2$ for $\epsilon = 0.1$ (see Fig. 11(a)) which just becomes more deep for the case of $\epsilon = 0.4$ (see Fig. 11(c)). The behaviour for the frequency of θ is rather more sensitive to the variation of ϵ. For $\epsilon = 0.1$ we see a hump around $\theta = \pi$ and two shallow valleys around $\theta = 1$ and $\theta = 5$, respectively. For $\epsilon = 0.4$ however, the behaviour is drastically changed. The hump around $\theta = \pi$ is now replaced by a constant plateau around the region of $\theta \in [2.5, 4]$. The two shallow valleys are now replaced by two deep valleys around $\theta = \pi/2$ and $\theta = 3\pi/2$. Thus, for $\epsilon = 0.4$ there are preferential regions on the phase plane that the particle visit with high frequency that were not observed for $\epsilon = 0.1$. Of course it accentuates regions that are also less visited as compared to the previous case. Such modifications in the phase space are assumed as the causes for the increase in the Lyapunov exponent.

4. Conclusion

As a conclusion, we have studied a classical version of a static oval billiard. We obtained the expressions of a two-dimensional nonlinear mapping that describe the dynamics of the model. We shown that the phase space has a mixed form. We have obtained an expression that relates both control parameters p and ϵ. We shown when $\epsilon > \epsilon_c$ the shape of the boundary changes from positive curvature to negative curvature and an important consequence of this changing is the sudden destruction of the invariant spanning curves in the phase space. The average angle α and its corresponding deviation were obtained as function of n. The behaviour of the positive Lyapunov exponent for the chaotic region was also obtained and discussed.

Acknowledgements

D.F.M.O. gratefully acknowledges CAPES. E.D.L. is grateful to FAPESP, CNPq and FUNDUNESP, Brazilian agencies. We also thanks Denis Gouvêa Ladeira and Douglas Fregolente for fruitful discussions.

Appendix

In this Appendix, we present the procedure to obtain the expression of the critical control parameter ϵ_c. When we increase the control parameter ϵ, the shape of the boundary changes (see Fig. 1). We can obtain the expression for the critical value ϵ_c, where the curvature of the boundary changes from positive ($\kappa > 0$) to negative ($\kappa < 0$). Using polar coordinates the expression for $\kappa(\theta)$ is given by

$$\kappa(\theta) = \frac{X'(\theta)Y''(\theta) - X''(\theta)Y'(\theta)}{[X'^2(\theta) + Y'^2(\theta)]^{\frac{3}{2}}}. \tag{17}$$

For the general case, the expressions for $X'(\theta)$, $Y'(\theta)$, $X''(\theta)$ and $Y''(\theta)$ are

$$\begin{aligned}
X'(\theta) &= \frac{dR(\theta)}{d\theta}\cos(\theta) - R(\theta)\sin(\theta),\\
Y'(\theta) &= \frac{dR(\theta)}{d\theta}\sin(\theta) + R(\theta)\cos(\theta),\\
X''(\theta) &= \frac{d^2R(\theta)}{d\theta^2}\cos(\theta) - 2\frac{dR(\theta)}{d\theta}\sin(\theta) - R(\theta)\cos(\theta),\\
Y''(\theta) &= \frac{d^2R(\theta)}{d\theta^2}\sin(\theta) + 2\frac{dR(\theta)}{d\theta}\cos(\theta) - R(\theta)\sin(\theta),
\end{aligned} \tag{18}$$

where $\frac{dR(\theta)}{d\theta}$ and $\frac{d^2R(\theta)}{d\theta^2}$ are given by

$$\begin{aligned}
\frac{dR(\theta)}{d\theta} &= \frac{(1-e^2)e\sin(\theta)}{[1+e\cos(\theta)]^2} - \epsilon p\sin(p\theta),\\
\frac{d^2R(\theta)}{d\theta^2} &= \frac{2(1-e^2)e^2\sin^2(\theta)}{[1+e\cos(\theta)]^3} + \frac{(1-e^2)e\cos(\theta)}{[1+e\cos(\theta)]^2} - \epsilon p^2\cos(p\theta).
\end{aligned} \tag{19}$$

We obtain ϵ_c by considering the case where $\kappa' = 0$. The expression for ϵ_c as function of e and p is

$$\epsilon_c = \frac{1-e}{(1+e)(1+p^2)}, \quad p > 1. \tag{20}$$

Thus, when $\epsilon < \epsilon_c$ the boundary is strictly convex, however, if $\epsilon > \epsilon_c$ we can observe nonconvex pieces on the boundary. For the case of $e = 0$ we recover the expression for ϵ_c obtained for the oval billiard.

References

[1] Birkhoff GD. Dynamical Systems Amer. Math. Soc. Colloquium Publ. 9. Providence: American Mathematical Society; 1927.
[2] Bunimovich LA. On ergodic properties of certain billiards. Funct Anal Appl 1974;8:254–5.
[3] Bunimovich LA. On the ergodic properties of nowhere dispersing billiards. Commun Math Phys 1979;65:295–312.
[4] Sinai YG. Dynamical systems with elastic reflections. Russ Math Surv 1970;25:137–89.
[5] Sinai YG. Ergodic properties of dispersive billiards. Russ Math Surv 1970;25:141–92.
[6] Berry MV. Regularity and chaos in classical mechanics, illustrated by three deformations of a circular billiard. Eur J Phys 1981;2:91–102.
[7] Kamphorst SO, de Carvalho SP. Bounded gain of energy on the breathing circle billiard. Nonlinearity 1999;12:1363–71.
[8] Robnik M. Classical dynamics of a family of billiards with analytic boundaries. J Phys A Math Gen 1983;16:3971–86.
[9] Robnik M, Berry MV. Classical billiards in magnetic fields. J Phys A Math Gen 1985;18:1361–78.
[10] Markarian R, Kamphorst SO, de Carvalho SP. Chaotic properties of the elliptical stadium. Commun Math Phys 1996;174:661–79.
[11] Lopac V, Mrkonjić I, Radić D. Chaotic dynamics and orbit stability in the parabolic oval billiard. Phys Rev E 2001;66:036202 (5pp).
[12] Lopac V, Mrkonjić I, Pavin N, Radić D. Chaotic dynamics of the elliptical stadium billiard in the full parameter space. Phys D 2006;217:88–101.
[13] Ozorio de Almeida AM. Hamiltonian systems: chaos and quantization. Cambridge: Cambridge University Press; 1988.
[14] Leonel ED, McClintock PVE, Scaling properties for a classical particle in a time-dependent potential well. Chaos 2005;15:033701–7.
[15] Mateos JL. Traversal-time distribution for a classical time-modulated barrier. Phys Lett A 1999;256:113–21.
[16] Luna-Acosta GA, Orellana-Rivadeneyra G, Mendoza-Galván A, Jung C. Chaotic classical scattering and dynamics in oscillating 1-D potential wells. Chaos Solitons Fractals 2001;12:349–63.
[17] Leonel ED, McClintock PVE. Chaotic properties of a time-modulated barrier. Phys Rev E 2004;70:016214 (11pp).
[18] Leonel ED, McClintock PVE. Dynamical properties of a particle in a time-dependent double-well potential. J Phys A Math Gen 2004;37:8949–68.
[19] Luna-Acosta GA, Mendez-Bermudéz JA, Seba P, Pichugin KN. Classical versus quantum structure of the scattering probability matrix: chaotic waveguides. Phys Rev E 2002;65:046605 (8pp).
[20] Luna-Acosta GA, Krokhin AA, Rodriguez MA, Hernandez-Tejeda PH. Classical chaos and ballistic transport in a mesoscopic channel. Phys Rev B 1996;54:11410–6.
[21] Ullmann K, Caldas IL. Symplectic mapping for the ergodic magnetic limiter and its dynamical analysis. Chaos Solitons Fractals 2000;11:2129–40.
[22] Portela JSE, Viana RL, Caldas IL. Periodic orbits and global chaos in a symplectic mapping describing magnetic field line structure in tokamaks. Phys A 2003;317:411–31.
[23] Da Silva EC, Caldas IL, Viana RL. Ergodic magnetic limiter for the TCABR. Braz J Phys 2002;32:39–45.
[24] Toporowicza LA, Beims MW. Correlation effects of two interacting particles in a circular billiard. Phys A 2006;37:5–9.
[25] Koiller J, Markarian R, Carvalho SP, Kamphorst SO. Static and time dependent perturbations of the classical elliptical stadium. J Stat Phys 1996;83:127–43.
[26] Eckmann JP, Ruelle D. Ergodic theory of chaos and strange attractors. Rev Mod Phys 1985;57:617–56.